




Comparative Analysis of Aerosol Direct Radiative Forcing During COVID-19 Lockdown Period in Peninsular India

Tharani Kotrike¹ · Venkata Reddy Keesara¹ · Venkataramana Sridhar²  · Deva Pratap¹

Received: 26 April 2023 / Accepted: 13 August 2024 / Published online: 1 September 2024
© The Author(s) 2024

Abstract

The load of aerosols in the atmosphere has been increasing gradually due to industrialization and urbanization. This increase has contributed to change in the Earth's radiation budget through the absorption or scattering of radiation. The aerosol direct radiative forcing (ADRF) is a measurement utilized to comprehend the impact of cooling or warming up of the atmosphere directly by aerosols. Our study examined the impact of aerosols during the COVID-19 pandemic by comparing them to the average from the preceding 5-year period (2015–2019) in peninsular India. The measure of aerosols deployed in this study is the Aerosol Optical Depth (AOD), and the study was carried out on three distinct time frames: prior to lockdown, during lockdown, and post lockdown. The study revealed that the ADRF increased during all the three time frames of 2020 compared to the average of 2015–2019, and the other time scales experienced an increase in ADRF as well. The most notable rise in ADRF and decrease in temperature occurred in the tropical savanna and warm semi-arid climate regions during the pre-lockdown period. During lockdown, the increase in ADRF was seen throughout the study area, and a decrease in temperature was observed only in the tropical monsoon region. In the post-lockdown period, the decline in ADRF was accompanied by a fall in temperature in the tropical savanna region. This study provides insights into the effect of aerosols on ADRF in peninsular India and highlights the importance of monitoring and regulating aerosol emissions to mitigate the changes in temperature.

Keywords Aerosol optical depth · Aerosol direct radiative forcing · COVID-19 lockdown period · India · Remote sensing · Temperature

Introduction

Solar radiation is a fundamental source of energy on Earth which is crucial for supporting the life and it drives many of the Earth's natural systems, including weather patterns, ocean currents, and the water cycle. However, the human activities, such as the emission of aerosols into the atmosphere, have affected the quantity of solar radiation that reaches the surface. The scattering of solar radiation by aerosols can cause a reduction in the amount of direct sunlight that reaches the surface, while the absorption of

radiation by aerosols can increase the amount of thermal energy in the atmosphere. This is one of the reasons why understanding the effect of aerosols on the Earth's climate is important. Human activities have the potential to alter the natural systems that sustain life on Earth by reducing the amount of solar radiation that reaches the surface (Liu et al., 2019, <https://ceres.larc.nasa.gov/>). In recent years, the number of anthropogenic aerosols in the atmosphere has increased significantly due to economic growth (Sarangi et al., 2016). These aerosols absorb and scatter the incoming solar radiation, which can alter the Earth's radiation budget (Mao & Wan, 2022). The impact of anthropogenic aerosols on solar radiation is of great importance because it affects the energy balance and hydrological cycle (Yang et al., 2018, Kumar et al., 2018; Sridhar et al., 2018; Valayamkunnath et al., 2018). Aerosols can influence the radiative flux at the Top Of the Atmosphere (TOA) and even more significantly at the surface through precipitation, which can impact biological processes (Sridhar & Anderson, 2017; Sehgal &

✉ Venkataramana Sridhar
vsri@vt.edu

¹ Department of Civil Engineering, National Institute of Technology, Warangal 506004, India

² Department of Biological Systems Engineering, Virginia Polytechnic Institute, State University, Blacksburg, VA 24061, USA

Sridhar, 2019; Setti et al., 2020a, b). While aerosols are found globally, their forcing effects are typically regional due to changes in climate, transport mechanism, deep convection etc. compared to the global forcing effects caused by greenhouse gases (GHGs) (Niyogi et al., 2007, Bellouin et al., 2020, Kumar et al., 2023).

The Aerosol Optical Depth (AOD) acts as a measure of extinction to solar radiation due to the absorption and scattering of the aerosols. In recent times, space-borne earth observation satellites have been used to understand aerosol properties on a global scale such as Scanning Imaging Absorption Spectrometer for Atmospheric Cartography (SCIAMACHY), Ozone Monitoring Instrument (OMI), Along Track Scanning Radiometer (ATSR), Multiangle Imaging Spectroradiometer (MISR), Total Ozone Mapping Spectrometer (TOMS), Advanced Very High Resolution Radiometer (AVHRR), Moderate Resolution Imaging Spectroradiometer (MODIS), UVN (UV–VISNIR) Spectrometer and Visible Infrared Imaging Radiometer Suite (VIIRS). The studies conducted on AOD obtained from most of the mentioned satellites have resulted in a reduction of AOD during the lockdown of 2020 in India (Rani et al., 2022).

The ADRF is a measurement utilized to comprehend the impact of cooling or warming up of the atmosphere directly by aerosols. The global radiative forcing due to aerosols has been negative over the past few decades. The presence of scattering aerosols leads to a reduction in the temperature of the planet by reflecting incoming solar radiation back into space while the absorbing aerosols tend to increase the temperature by absorbing the solar radiation. This is different from greenhouse gases, which traps the heat in the atmosphere and leads to an increase in temperature. The magnitude of the radiative forcing due to aerosols is still uncertain and under investigation (Shonk et al., 2020). The most widely used method for estimating ADRF is to incorporate parameters from Moderate Resolution Imaging Spectrometer (MODIS), Clouds and Earth's Radiant Energy System (CERES) in Santa Barbara DISORT Atmospheric Radiative Transfer (SBDART) model. The estimates of the net radiative forcing due to aerosols are uncertain because of various factors that influence how aerosols interact with incoming solar radiation (Pandey et al., 2020, Mao & Wan, 2022). The heterogeneity of aerosol distribution can lead to spatio-temporal variations in radiative effects across different locations. The distribution of aerosols with altitude can also affect how much solar radiation they intercept and reflect. Additionally, different aerosol species have different optical properties, and their relative contributions to the ADRF affects the overall net radiative forcing. These factors can all lead to uncertainties in the estimates of the net radiative forcing due to aerosols (Subba et al., 2020). To improve the reliability of ADRF estimates, researchers have combined model studies in-situ measurements and remote

sensing observations (Paulot et al., 2018; Putaud et al., 2014; Zhang et al., 2005). ADRF has been found to increase by 0.7–1 W/m² in Western Europe and 0.9–1.4 W/m² in Eastern America. However, a decrease of 1–1.6 W/m² in ADRF has been observed in India over the period of 2001–2015 (Paulot et al., 2018).

Modeling research has shown that the temperature tends to decrease when there are aerosols in the atmosphere (Wang et al., 2017). However, the type of aerosol can change the cooling and warming pattern of an area. The emissions of black carbon leads to the absorption of radiation and a rise in the temperature which in turn results in the annihilation of clouds. The scattering of radiation results in the radiative cooling of the atmosphere. The impact of aerosols on the Earth's climate can be particularly pronounced in regions with high emissions of sea-salt aerosols. Accurate evaluation of the radiative forcing resulting from aerosols and its influence on Earth's climate is crucial (Jaksa et al., 2013; Lopez et al., 2021, Rosenfield et al., 2008, Sridhar & Wedin, 2009, Yu et al., 2006).

Corona Virus Disease (COVID-19) is an infectious disease caused by the Severe Acute Respiratory Syndrome Corona Virus 2 (SARS-CoV-2) (Gauda et al., 2022). The disease's global spread in late 2019, originating in China, has resulted in a catastrophic loss of human life. The World Health Organization (WHO) declared COVID-19 a pandemic on March 12, 2020, leading many countries to impose restrictions on industrial activities and human movement. The Indian government implemented a nationwide shutdown on March 24, 2020, resulting in a lockdown from March to May 2020. Moreover, the lockdown has resulted in pristine sky conditions in many parts of the world, providing researchers with an opportunity to study air quality and its impact on climate variables (Thomas et al., 2021; Thomas et al., 2022).

Researchers worldwide have investigated the impact of the lockdown on various atmospheric parameters across regions, including South Asia (Li & Tartarini, 2020; Navinya et al., 2020, Sahu et al., 2022), Europe (Tobias et al., 2020), North and South America (Zalakeviciute et al., 2020). Studies have shown that the air quality has improved significantly due to industrial and vehicular restrictions. The presence and quantity of aerosols in the atmosphere play a crucial role in understanding air quality.

Previous studies were performed to know the effect of aerosols on the radiative budget has been studied under clear sky conditions (Subba et al., 2020, Thomas et al., 2021). The objective of this study is to evaluate the impact of aerosols on radiation at the top of the atmosphere, the surface, and in the atmosphere, under all sky conditions. Furthermore, as noted by Rani and Kumar (2022) and Gauda et al. (2022), there has been a dearth of research examining the impact on air temperature resulting from alterations in aerosol levels

during the lockdown period in India. The longwave fluxes without aerosols are not available from MERRA-2 data. They are estimated by the factored method as coined by the authors. The uniqueness of this paper lies in the computation of ADRF in all-sky conditions by utilizing the accessible and estimated fluxes. The trend in ADRF in the atmosphere is studied using the non-parametric Mann–Kendall test for the time period of 2015–2019. The Aerosol Optical Depth, ADRF, and mean temperature are evaluated from 2015–2020. The spatial distribution of these parameters in 2020 is compared to the average of 2015–2019 for three analysis periods in order to understand the direct effect of the COVID-19 lockdown on the spread of aerosols and the indirect impact on temperature through changes in ADRF.

Study Area

The current study focuses on the Peninsular Indian region, which consists of nine states: Maharashtra, Orissa, Chhattisgarh, Goa, Andhra Pradesh, Telangana, Karnataka, Tamil Nadu, and Kerala. Recent research indicates that the concentration of aerosols in the atmosphere has

grown, delaying the start of the south-west monsoon season, which is a significant source of rainfall in the area (Sarangi et al., 2016, Niyogi et al., 2007). Agriculture is the primary economic source in this region, while income from small and medium scale industries is the secondary source of livelihood for many people. The terrestrial region of Peninsular India considered for the study has an area of 1239 lakh ha. Nearly, 40% of India's population lives in the chosen study area. The area is bound by the Indian Ocean to the South, the Bay of Bengal to the East, the Arabian Sea to the West, Vindhya and Satpura region to the North. The geography of the study area comprises the Deccan Plateau, Western and Eastern Ghats.

Previous research has largely focused on the Himalayan region and central India when studying Aerosol-Radiation Interactions (ARI). This study aims to understand the phenomenon in a different, terrestrial region with varying climates, and to assess the effect of ARI on the region. The climatic zones according to Koppen's Classification for the study area are Tropical Savanna climate (Aw), Monsoon climate (Am), Warm Semi-arid climate (BSh), Humid Subtropical climate (Cwa) and Subtropical Oceanic Highland climate (Cwb) (Fig. 1).

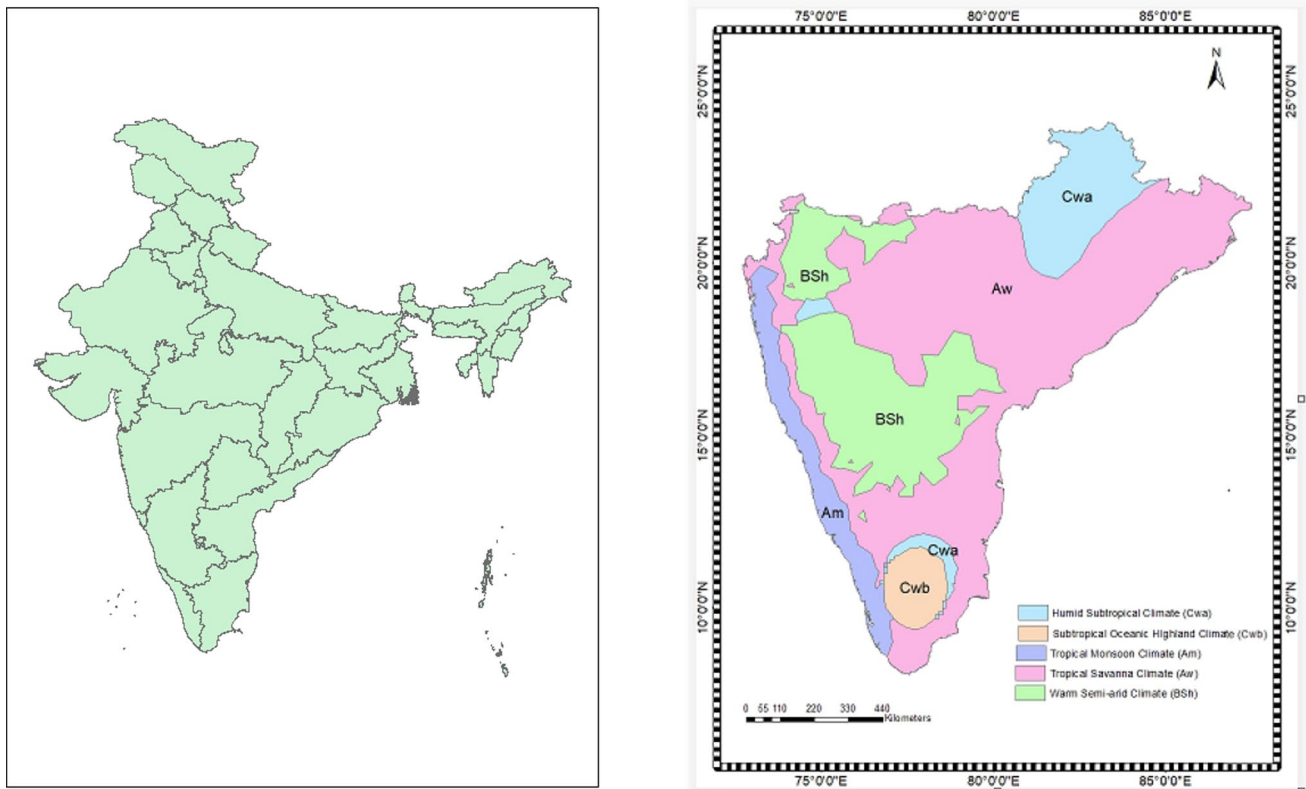


Fig. 1 Location map of study area with Koppen's climate zones

Data

The data used in this study was a combination of satellite, model re-analysis Aerosol Optical Depth (AOD) data and Indian Meteorological Department (IMD) gridded temperature data. AOD data is collected daily by MODIS (Moderate Resolution Imaging Spectroradiometer) onboard with Terra and Aqua satellites which is monitored by NASA. The Terra satellite collects data at 10:30 local hours, and the Aqua satellite collects data at 13:30 local hours. (<https://modis.gsfc.nasa.gov>). The MODIS data uses the Dark Target algorithm and the Look Up Table procedure to estimate the spectral information of aerosols over land surfaces in the visible wavelength region at a spatial resolution of 10 km. The calculation of Aerosol Optical Depth (AOD) from satellite radiances involves using the Angstrom exponential law, which is a mathematical relationship between the AOD and the scattering properties of aerosols. The AOD at 550 nm is determined by using the sensor's input of the radiation flux recorded at 470 and 670 nm wavelengths from MODIS. The uncertainty in the retrieval of MODIS AOD over the land is $\pm 0.05 \pm 0.15 \tau$ (Remer et al., 2005) where τ is AOD at 550 nm. The high spatial resolution allows for a detailed assessment of the distribution of aerosols over the Earth's surface (Kotrike et al., 2021), which is essential for understanding the aerosol radiative forcing and its impact on the Earth's climate.

The Modern-Era Retrospective analysis for Research and Applications (MERRA-2) is a NASA's atmospheric reanalysis that provides a long-term, consistent, and high-resolution dataset of various atmospheric variables, including radiation fluxes. The MERRA-2 reanalysis has been upgraded using the Goddard Earth Observing System Model, (GEOS-5) Version 5 data assimilation system. This improved the accuracy and resolution of the dataset (Rienecker et al., 2011). The MERRA-2 dataset is widely used in a variety of research fields, including climate studies, weather forecasting, and air quality assessments. The radiation fluxes obtained from the MERRA-2 reanalysis provide a comprehensive view of the energy balanced in the atmosphere and the surface and can be used to better understand the impacts of human activities and climate change on atmospheric temperature and radiation fluxes. The use of the MERRA-2 dataset in this study provides a valuable source of information for understanding the relationship between the aerosol optical depth and radiation fluxes. The net shortwave and longwave fluxes can be found in the M2T1NXRAD_5.12.4 data set of MERRA-2, and are available at a resolution of $0.5^\circ \times 0.625^\circ$. The uncertainty in the flux estimates of MERRA-2 is in the range of 4–6% (Buchard et al., 2017).

Indian Meteorological Department (IMD) Gridded Temperature Data

High-resolution temperature datasets allow for the analysis of extreme climate conditions from the past. One such dataset is provided by the Indian Meteorological Department (IMD) located in Pune, India. The IMD operates 550 observatories where daily maximum and minimum surface air observations are recorded. These observations are then processed using Shepard's angular distance weighing algorithm and converted into $1^\circ \times 1^\circ$ gridded locations. The IMD currently offers data from 1969 to 2020 (Srivatsava et al., 2009).

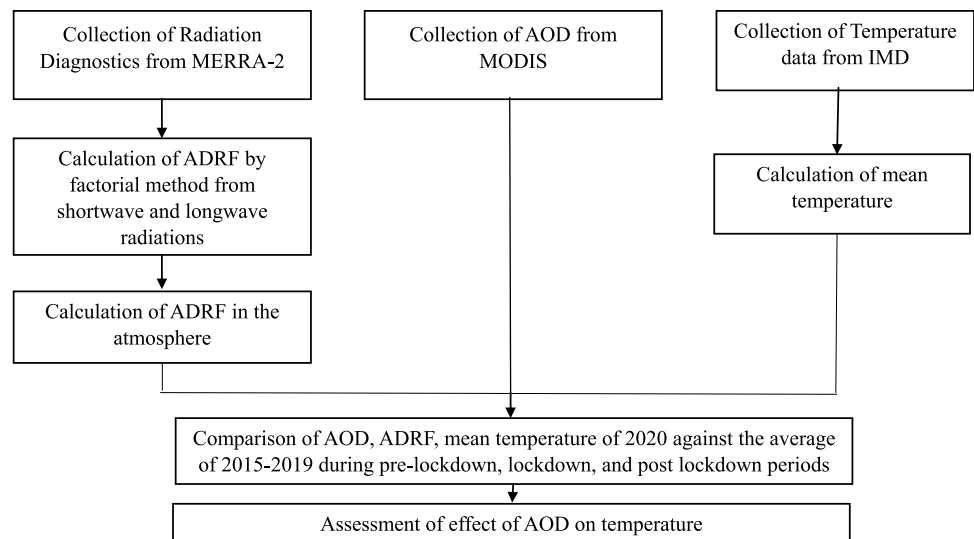
Methodology

The methodology adopted in this study is illustrated in Fig. 2. The initial step is to calculate the ADRF at the Top of the Atmosphere ($ADRF_{TOA}$), at the Surface ($ADRF_{SUR}$), and in the atmosphere ($ADRF_{ATM}$) using MERRA-2 radiation flux data under all-sky conditions. The second step is to analyze the trend in ADRF over the period of 2015–2019 using the Mann–Kendall analysis method. The third step is to compare the averaged observations against the COVID impacted year i.e. 2020. Three analysis periods are considered for the study namely Period 1 (January 1 to March 23) which is pre-lockdown in 2020, Period 2 (March 24 to May 31) which is lockdown in 2020 and Period 3 (June 1 to August 31) which is post-lockdown in 2020. The average of observations (AOD, ADRF, Temperature) for the duration of 2015–2019 over the abovementioned three analysis periods is calculated. The comparison of averaged observations for the three analysis periods with the corresponding three analysis periods of 2020 is performed to understand the influence of AOD on radiation budget. The final step is to assess the effect of AOD on temperature for each Koppen's climatic zone in the study area for the three analysis periods.

Calculation of Aerosol Direct Radiative Forcing (ADRF)

The ADRF (Aerosol Direct Radiative Forcing) calculation requires several parameters, including the Surface Net Downward Shortwave Flux (SWGNT), the Surface Net Downward Shortwave Flux assuming no aerosol (SWGNTCLN), the Surface Net Downward Longwave Flux (LWGNT), the Surface Net Downward Longwave Flux assuming no aerosol (LWGNTCLN), the TOA Net Downward Shortwave Flux (SWTNT), the TOA Net Downward Shortwave Flux assuming no aerosol (SWTNTCLN), the Upwelling Longwave Flux at TOA (LWTUP), and the Upwelling Longwave Flux at TOA assuming no

Fig. 2 Methodology for assessing the effect of AOD on radiation budget and temperature



aerosol (LWTUPCLN). While six of these parameters can be directly obtained from MERRA-2, the LWGNTCLN and LWTUPCLN need to be calculated. The following equations are generally used to calculate the ADRF at the surface (Eq. 1) and at TOA (Eq. 2).

$$ADRF_{SUR} = (SWGNT + LWGNT) - (SWGNTCLN + LWGNTCLN) \tag{1}$$

$$ADRF_{TOA} = (SWTNT + LWTUP) - (SWTNTCLN + LWTUPCLN) \tag{2}$$

The atmospheric ADRF ($ADRF_{ATM}$) is calculated by subtracting the ADRF at the surface from the ADRF at the top of the atmosphere (TOA). According to standard conventions, a positive $ADRF_{ATM}$ warms the atmosphere while a negative $ADRF_{ATM}$ cools it. The current study aims to determine the missing parameters using two methods: the factored method and the difference method. The factored method involves dividing $SWGNTCLN$ by $SWGNT$ to obtain a factor, which is then used to calculate $LWGNTCLN$ using Eq. (3). The difference method, on the other hand, uses the difference between $SWGNTCLN$ and $SWGNT$ to calculate $LWGNTCLN$ using Eq. (4).

$$LWGNTCLN_f = \frac{SWGNTCLN}{SWGNT} * LWGNT \tag{3}$$

$$LWGNTCLN_d = SWGNTCLN - SWGNT + LWGNT \tag{4}$$

Five grid points, one in each climate zone of the study area are considered. The grid points chosen are Goa falls in Am, Nanded falls in Aw, Hyderabad falls in BSh, Raipur falls in Cwa, and Coimbatore falls in Cwb climate zones. The time series of long wave flux data of 2019, calculated using both the factored and difference methods was plotted.

Trend in ADRF

The non-parametric Mann–Kendall test is a widely used statistical method for analyzing trends in time series data. The test is used to determine if there is a monotonic trend in the data, without making any assumptions about the underlying distribution of the data. The test first calculates the S statistic shown in Eq. 5 (Mann, 1945, Kendall, 1975), which represents the sum of the differences between the data points, and then uses this value to calculate the *p*-value, which represents the significance of the trend.

$$S = \sum_{a=1}^{n-1} \sum_{b=a+1}^n sgn(x_b - x_a) \tag{5}$$

In this equation, x_b represents the observed value at time *b*, while x_a represents the observed value at time *a*. It is important to note that *a* should be less than *b*, and *n* represents the total amount of data points in the set. The sign of the value is determined according to Eq. 6, as proposed by Mann (1945) and Kendall (1975).

$$sgn(x_b - x_a) = \begin{cases} 1 & \text{if } (x_b - x_a) > 0 \\ 0 & \text{if } (x_b - x_a) = 0 \\ -1 & \text{if } (x_b - x_a) < 0 \end{cases} \tag{6}$$

The test's multiple trials showed that the S statistic follows a normal distribution with a mean equal to Eq. 7 and a variance equal to Eq. 8 when the number of samples are greater than 8. (Mann, 1945, Kendall, 1975).

$$E(S) = 0 \tag{7}$$

$$\text{Var}(S) = \frac{n(n-1)(2n+5) - \sum_{i=1}^r t_p(t_p-1)(2t_p+5)}{18} \quad (8)$$

where i indicates the number of measurements, r indicates the number of groups of data points with the same value in the time series data and the value of t represents the number of data points with the same value in the p th group. The Z score is used to check the statistical significance of S . The Z statistic follows a normal distribution with zero mean and unit variance as shown in Eq. (9) (Chakraborty et al., 2011).

$$Z = \begin{cases} \frac{s-1}{\sqrt{\text{var}(s)}}; S > 0 \\ 0; S = 0 \\ \frac{s+1}{\sqrt{\text{var}(s)}}; S < 0 \end{cases} \quad (9)$$

The Mann–Kendall method is used to test whether there is a trend in a set of data. The hypothesis that there is no trend is denoted as null hypothesis H_0 whereas the hypothesis that there is presence of trend is considered as alternative hypothesis H_1 . The null hypothesis is rejected based on the two-tailed test. The Z test statistic value is used to test H_0 . If Z is negative, it indicates a decreasing trend, and if it is positive, it indicates an increasing trend. In this study, the hypothesis is tested at a confidence level of 95%. The slope of the trend in dataset is calculated by linear regression method. The magnitude of the change in the ADRF data is also determined using Sen's method, which offers insight into the data's rate of change over time. Since the Mann–Kendall method does not assume any underlying distribution for the data, it can be applied to the assessment of a broad variety of time series data. In this study, the magnitude of the trend in time series data is estimated using Eq. 10.

$$Q_i = \frac{x_b - x_a}{(b - a)} \quad (10)$$

The present study incorporates the Mann–Kendall test to test the trend of Q_i , which is the slope between data points x_b and x_a . The test was performed using the *spatialEco* and *raster* packages in R software (Evans et al., 2019).

Effect of Aerosols on Temperature

To understand the impact of aerosols on the Earth's radiation budget, the changes in temperature due to the presence of aerosols is analysed for each climate zone in the study area. The annual mean temperature and the annual average daily radiation flux for the year 2020 and the average of the years 2015–2019 are calculated for the study area. The comparison is then made between the year 2020, which was impacted by the COVID-19 pandemic, and the average of the years 2015–2019 over three analysis periods.

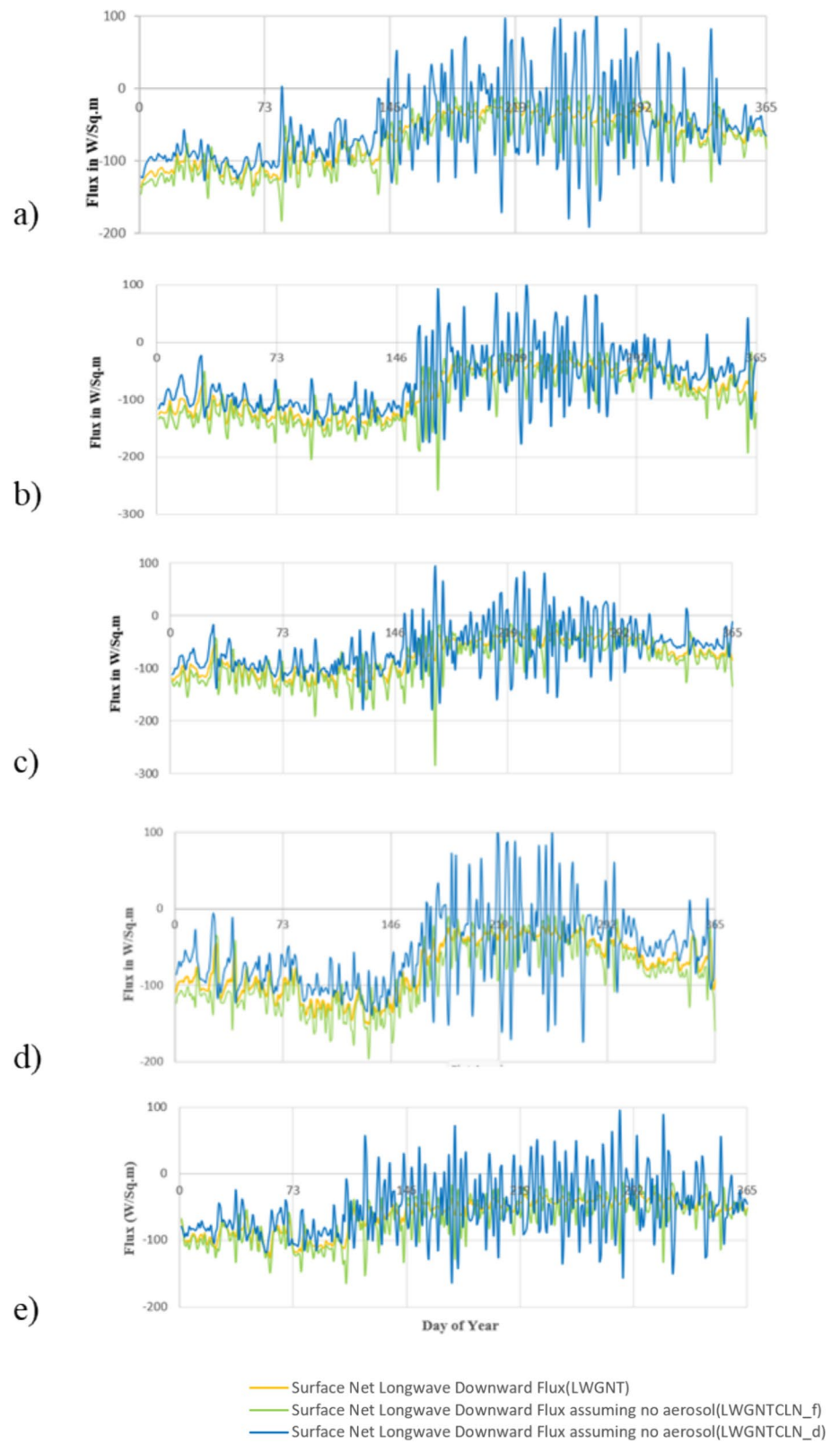
The methodology discussed in Sect. "Methodology" was applied to the study area chosen for the research. The results obtained are discussed as follows.

Results and Discussions

Calculation of ADRF

The estimated ADRF time series plot for all five grid points is depicted in Fig. 3. The flux is higher in most of the monsoon and post-monsoon seasons for all the five chosen grid points in the study area. This might be due to the accumulation of aerosols under favourable conditions of atmosphere during these seasons (Mohanty et al., 2002). The overall flux in the year 2019 ranged from -200 W/m^2 to 100 W/m^2 . It can be seen that the LWGNTCLN calculated using the factored method follows a similar pattern to that of the LWGNT. The location of peaks and dips in LWGNTCLN exactly matches that of LWGNT in all the grid points. However, while the peaks and dips of the LWGNTCLN calculated using the difference method align with those of the LWGNT, the disparity in the amount of flux appears to be significant (Fawole et al., 2019). The data for the grid points from the five different climate zones show a resemblance in their time series plots. The LWGNT for Goa (Fig. 3a) is in the range of -180 to -9.5 W/m^2 . The LWGNTCLN by factored and difference method for Goa is in the range of -135 to -21 W/m^2 and -188 to 115 W/m^2 , respectively. The minimum value of LWGNTCLN_d is close to LWGNT, whereas the maximum value is higher than that of LWGNT. The LWGNT, LWGNTCLN_f, and LWGNTCLN_d for Nanded (Fig. 3b) are between -153 to -25 , -254 to -10 , and -175 to 101 W/m^2 , respectively. From Fig. 3b, it is evident that the occurrence of the dip matches for LWGNTCLN_f, but the values at those particular locations are lower than that of LWGNT. On the other hand, the values at peaks are near to that of LWGNT. The LWGNT, LWGNTCLN_f, and LWGNTCLN_d for Hyderabad (Fig. 3c) are between -138 to -24 , -282 to -9 , and -178 to 94 W/m^2 , respectively. Although the pattern of LWGNTCLN_d matches that of the LWGNT, the flux values appear to be higher, and the distribution is vague when compared to that of the LWGNT. The values at dips are on a higher note for LWGNTCLN_f, but they are on par at peaks with respect to the LWGNT. The LWGNT, LWGNTCLN_f, and LWGNTCLN_d for Raipur (Fig. 3d) are between -150 to -20 , -196 to -7 , and -173 to 102 W/m^2 , respectively. The pattern and distribution are the same as those of the other three locations. The LWGNT, LWGNTCLN_f, and LWGNTCLN_d for Coimbatore (Fig. 3e) are between -127 to -25 , -165 to -14 , and -164 to 95 W/m^2 ,

Fig. 3 Time series plot of LWGNT, LWGNTCLN_f, LWGNTCLN_d for **a** Goa, **b** Nanded, **c** Hyderabad, **d** Raipur, **e** Coimbatore for the year 2019



respectively. The values at dip locations are lower for LWGNTCLN_f and LWGNTCLN_d, but the values of LWGNTCLN_f at peak locations are on par with LWGNT and that of LWGNTCLN_d are higher. On the whole, it can be said that LWGNTCLN obtained by the factored method appears to be in consonance with LWGNT.

Trend in ADRF

Over the period of 2015–2019, the trend in ADRF in the atmosphere was calculated using the non-parametric Mann–Kendall test as described in Sect. 3.2. The IPCC 2013 report concentrates on the reduction in anthropogenic emissions (Woodward et al., 2014). Most of the countries have deployed the suggested measures to reduce the emissions. The reduction in emissions generally leads to a reduction in the absorption and scattering of radiation which in turn is related to ADRF. Therefore, the trend in ADRF is calculated for 2015–2019 after the implementation of measures to reduce the anthropogenic emissions. The magnitude of the trend at a 5% significance level was then determined using the Sen's slope formula, which divides the magnitude into four classes: very low positive change, low positive change, moderate change, and high change. Most of the study area exhibited a low positive change in ADRF as shown in Table 1 for the different climatic zones. The areas experiencing very low positive change and high change were roughly equal in the tropical monsoon (Am) climate zone. This may be due to the sea-salt emissions from coastal region in different seasons of a year. The trend in ADRF during 2015–2019 in the tropical savanna (Aw) climate region showed a very low positive change, followed by moderate and high changes. The area with high change is more in Aw. This might be due to the industrial emissions in that time period. The humid subtropical climate (Cwa) exhibited low and moderate positive changes significantly. The subtropical oceanic highland climate (cwb) region showed only a very

Table 1 Area of significant change in ADRF for each climate zone (in lakh hectares)

Climate zone	Change in ADRF			
	Very low positive change	Low positive change	Moderate change	High change
Am	13.42	41.30	19.07	13.90
Aw	104.28	328.26	97.67	33.73
BSh	64.50	166.00	38.72	–
Cwa	9.78	74.66	49.16	0.67
Cwb	39.78	2.20		

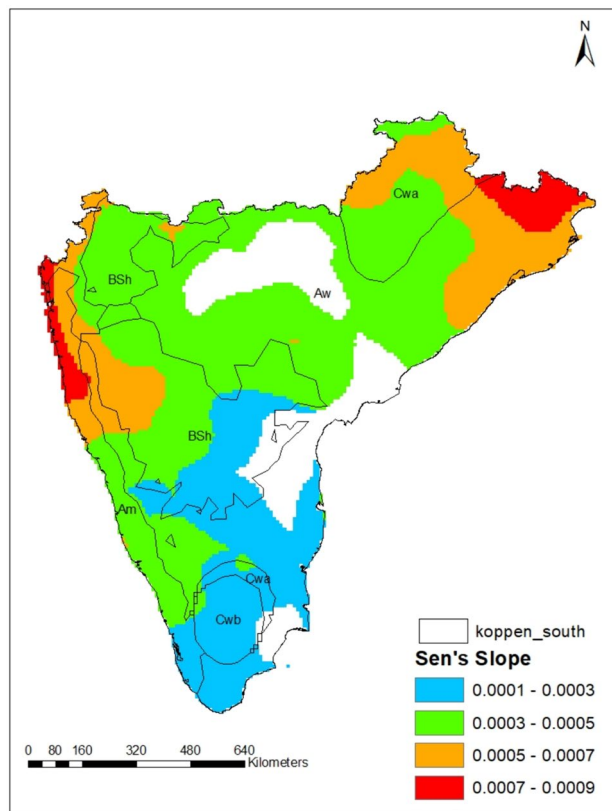


Fig. 4 Spatial distribution of trend in ADRF

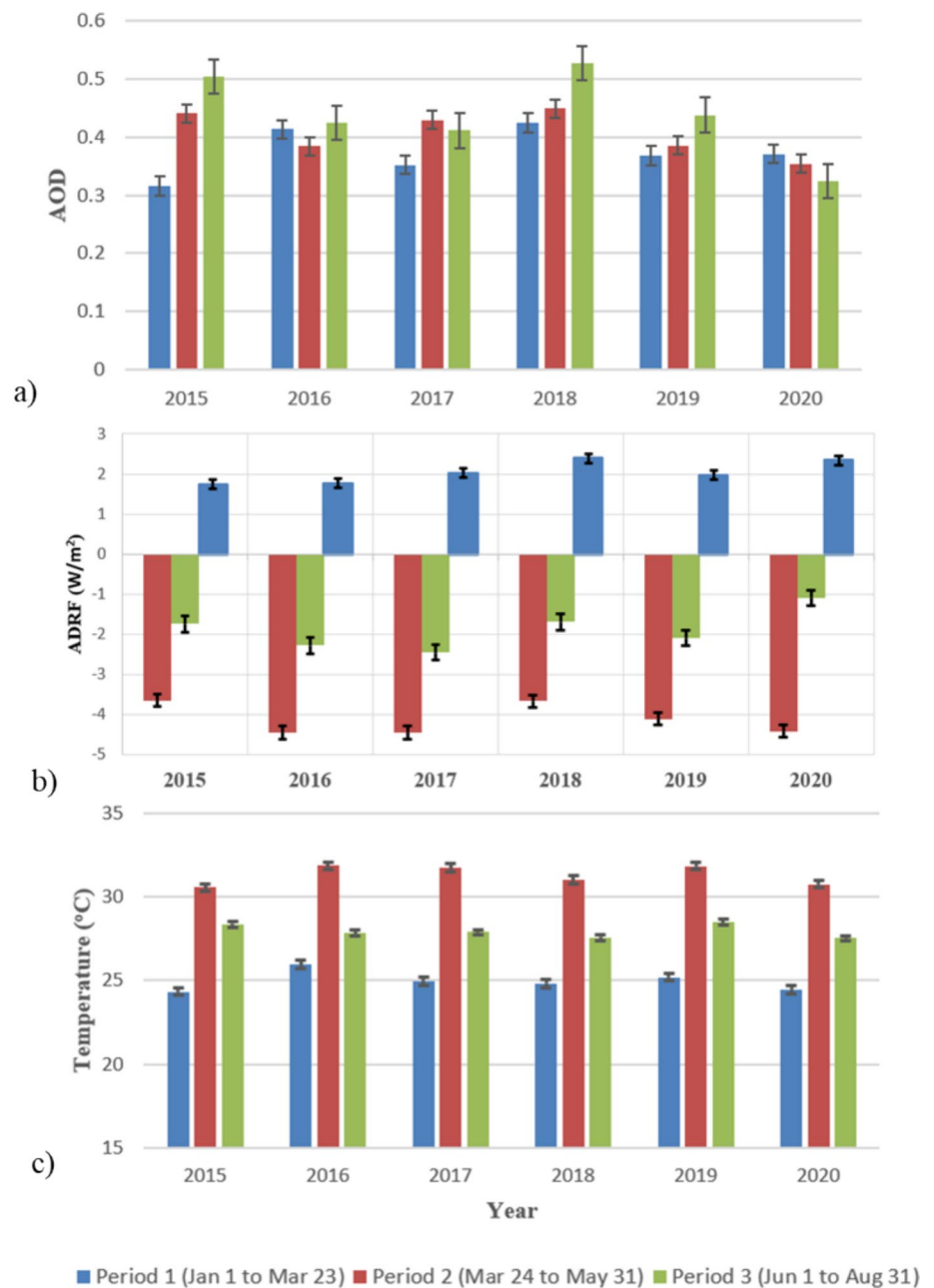
low positive change in the trend. The trend in ADRF is depicted in Fig. 4.

Variations in AOD, ADRF, and Temperature During Pre-Lockdown, Lockdown, and Post-Lockdown Periods

The variations in AOD, ADRF, and temperature for the period of 2015–2020 over the three analysis periods are shown in Fig. 5. The error bar in the figure represents the standard error in the parameter considered during that particular period of each year. The AOD in all three analysis periods was found to be maximum in the year 2018 (0.425, 0.449, and 0.526) (Fig. 5a). This might be due to an increase in the emissions that are entrapped in the column of the atmosphere. The average AOD during 2015–2019 in Period 1 was ~0.7, while it was ~0.6 in the year 2020. The AOD in the Period 2 of the year 2020 also decreased by ~0.1 compared to the average of the past five years (2015–2019). On the contrary, a significant increase of about ~0.8 was seen in the Period 3 of the year 2020 when compared to the mean of the period 2015–2019. Similar observations were recorded by Pandey et al. (2020).

Figure 5b corresponds to the variation of ADRF over the period 2015–2020. The ADRF in the months of January

Fig. 5 Variation of parameters over the duration of 2015–2020 in three analysis periods **a** AOD, **b** ADRF, **c** Temperature (Error bar represents standard error in the parameter considered during analysis period of each year)



to March of the years 2016, 2017, and 2020 was almost the same and had low values. The period March–May of 2017 (which is the lockdown period in 2020) has seen a lower ADRF of -2.49 W/m^2 , while the highest was in the year 2020 with a value of -1.09 W/m^2 . This may be due to the higher amount of radiation reaching the Earth's surface, which results in higher radiative forcing in the atmosphere. The Period 3 of the year 2020 witnessed a higher ADRF of 2.34 W/m^2 , which is close to that seen in the year 2018 (2.39 W/m^2). The Period 3 has seen a positive ADRF which is in accordance to the increase in AOD over the same time scale (Subba et al., 2020).

Figure 5c shows the variation of temperature over the period 2015–2020. The temperature ($25.96 \text{ }^\circ\text{C}$) in the period of January 1 to March 23 of 2016 (which is the pre-lockdown period of 2020) was found to be the highest. In the year 2019, the temperature in the periods March 24 to May 31 (lockdown period in the year 2020) and June 1 to August 31 (post-lockdown period in the year 2020) was $31.85 \text{ }^\circ\text{C}$ and $28.49 \text{ }^\circ\text{C}$, respectively. These were the highest values over a period of 2015–2020. The temperature was minimum in all three analysis periods of 2020 when compared to the past five-year data. This is in good agreement with the annual report of 2020 provided by the

Indian Meteorological Department (<https://mausam.imd.gov.in>).

COVID-19 Lockdown: Pristine Situation

The COVID-19 pandemic that began at the end of 2019 has led to a complete shutdown of industrial and human activities in India from March 24, 2020 to May 31, 2020. During this time, there was a notable decrease in the accumulation of aerosols in the atmosphere worldwide (Muhammad, et al., 2020; Singh & Chauhan, 2020). This decrease was also seen in satellite data from MODIS. To understand the impact of aerosols on temperature in a normal situation, the average of all variables for each of the three analysis periods during 2015–2019 were also analyzed.

Spatial Distribution of AOD in the Atmosphere

The spatial distribution of aerosol optical depth (AOD) in the study area is shown in Fig. 6. According to research conducted by Thomas et al. (2021), the aerosol loading has decreased during the lockdown period in the study area. In fact, about 56% of the study area saw a decrease in AOD during the pre-lockdown period of 2020 compared to the average from 2015–2019. This decrease in AOD was upto 0.43, while the increase fluctuated from 0 to 0.48 which is in accordance with the results exhibited by Rani et al. (2022). The majority of the decrease was observed in the tropical monsoon (Am) region covering Goa and the humid subtropical region (Cwa) covering cities like Chennai and Bengaluru. On the other hand, the increase was predominantly seen in and around cities such as Pune and Mumbai belonging to

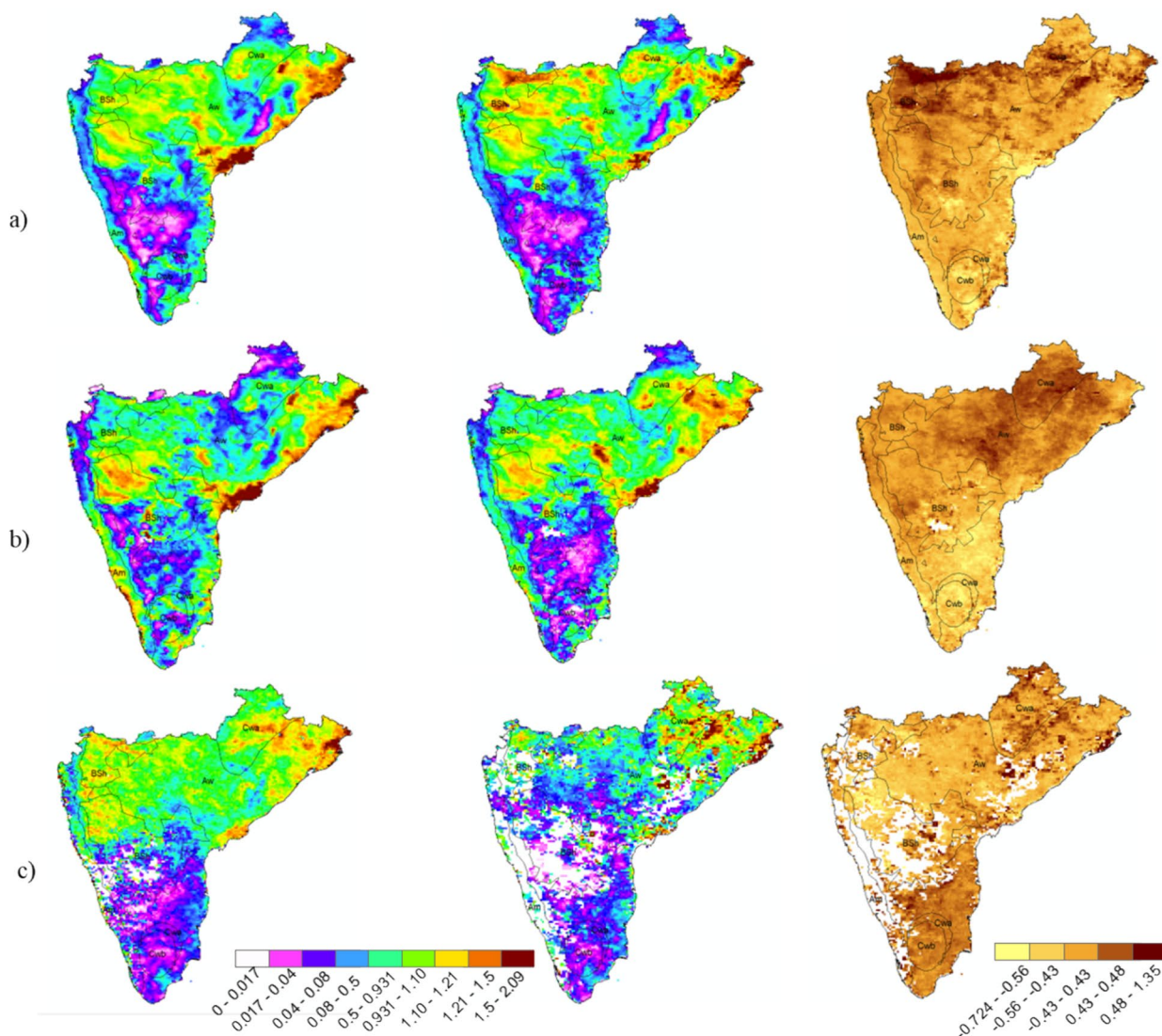


Fig. 6 Spatial distribution of AOD for **a** Period 1, **b** Period 2, **c** Period 3 (Left: average of 2015–2019, Middle: 2020, Right: Change)

the tropical savanna region (Aw) and Hyderabad belonging to the warm semi-arid region (BSh).

During the Period 2, the spatial distribution of AOD shows that 15% of the area had an increase in AOD was upto 0.43, primarily in the subtropical oceanic highland climate region (Cwb) which is in accordance with the results given by Gaouda et al. (2022). The decrease in AOD was distributed in the tropical savanna (Aw) regions, which includes metropolitan cities like Chennai, Mumbai, and Bengaluru and warm semi-arid climate region (BSh) which is predominant in city like Hyderabad. In the Period 3, there was a decrease in AOD that stretched from 0 to 0.72, while the increase ranged from 0 to 1.35. The distribution indicates that the decrease was observed in parts of the tropical savanna (Aw) region with metropolitan cities like Chennai, Bengaluru and Mumbai, while the increase was seen in parts of the humid subtropical climate region (Cwb).

Spatial Distribution of ADRF in the Atmosphere

The reduction in aerosol loading has resulted in a downfall in ADRF in the atmosphere (Thomas et al. 2021, Subba et al., 2020). The ADRF in the atmosphere for the year 2015 was $-1.5 \pm 0.006 \text{ W/m}^2$, and in 2019, it was $-1.42 \pm 0.005 \text{ W/m}^2$. Over a period of five years, there has been an atmospheric warming of $0.08 \pm 0.001 \text{ W/m}^2$, which is in accordance with Rutan et al. (2015). The ADRF in Period 1 for the year 2015 was $-3.64 \pm 0.007 \text{ W/m}^2$, and in 2019, it was $-4.10 \pm 0.008 \text{ W/m}^2$. However, the average ADRF (2015–2019) for pre-lockdown lies closer to that of 2019 with a value of $-4.06 \pm 0.009 \text{ W/m}^2$. The ADRF was lower in most of the Aw region and high in the BSh region (Fig. 6). The ADRF in the atmosphere during the Period 2 for the year 2015 was $-1.74 \pm 0.009 \text{ W/m}^2$, and in 2019, it was $-2.09 \pm 0.006 \text{ W/m}^2$. The ADRF was low in the northern parts of warm semi-arid (BSh) and high in the southern parts of the warm semi-arid (BSh) region in the study area. Atmospheric warming is observed in the Period 3 with $1.74 \pm 0.004 \text{ W/m}^2$ (2015) and $1.97 \pm 0.003 \text{ W/m}^2$ (2019). The average ADRF in Period 3 is found to be $1.98 \pm 0.007 \text{ W/m}^2$. The spatial distribution shows that the lower values are towards the tropical monsoon (Am) and sub-tropical oceanic highland (Cwb) regions, while higher values are in the warm semi-arid (BSh) and tropical savanna (Aw) climate regions. The distribution might be attributed to the occurrence of monsoon precipitation and the trapping up of heat due to the dispersion of clouds without precipitation (Das et al., 2015, Cheng et al., 2017). The ADRF during the three analysis periods of 2020 is found to be -4.41 ± 0.06 , -1.09 ± 0.04 , and $2.34 \pm 0.02 \text{ W/m}^2$, respectively. It is observed to have an atmospheric warming of approximately 0.4 W/m^2 in the Period 3 of 2020 compared to the average of 2015–2019 which is in accordance with Srivastava et al.

(2021) and Thomas et al. (2022). This may be due to the dilution of aerosols in the atmosphere or the excess formation of cloud condensation nuclei.

According to Fig. 7, nearly 74% of the study area experienced a decrease in ADRF during the Period 1 of 2020 compared to the average of 2015–2019. The decrease in ADRF ranged from 0 to 1.7 W/m^2 , while the increase in the remaining 26% of the study area ranged from 0 to 0.83 W/m^2 . The decrease was more prominent in tropical savanna (Aw) and in warm semi-arid (BSh) regions. In contrast, the increase was seen in humid regions and a part of the tropical monsoon region. However, the situation changed drastically during the Period 2. Almost 98% of the study area showed an increase in ADRF during the lockdown of 2020 compared to the average of 2015–2019. The rise in ADRF fluctuated between 0 and 2.32 W/m^2 , while the fall fluctuated between 0 and 0.23 W/m^2 . The spatial distribution of ADRF shows that the increase was distributed across all five climate zones of the study area, but the decrease was concentrated only in the coastal part of the tropical savanna region. A part of the fall was also distributed to the humid subtropical region. During the Period 3, nearly 93% of the study area experienced an increase in ADRF ranging from 0 to 1.21 W/m^2 , while the remaining part saw a decrease in ADRF ranging from 0 to 0.21 W/m^2 . The reduction in ADRF was seen in most of the western and eastern ghats, while the increase was seen in the landlocked part of the study area. The decrease in the coastal parts of the tropical monsoon and savanna regions might be attributed to the onset of the south-west monsoon season.

Spatial Distribution of Temperature in the Atmosphere

Theoretically, temperature is supposed to follow the trend of ADRF. The average temperature in the Period 1 of 2019 in the study area was $25.20 \pm 0.005 \text{ }^\circ\text{C}$, which is higher than that of 2015 ($24.34 \pm 0.006 \text{ }^\circ\text{C}$). The increase in temperature during the Period 2 between 2015 and 2019 was $\sim 1.3 \text{ }^\circ\text{C}$, which is contrary to the context of ADRF. From the analysis, ADRF during the abovementioned two periods was found to result in the cooling of the atmosphere, but the temperature did not follow the pattern of ADRF (Irfan et al., 2022). This might be due to the formation of aerosol nuclei that support cloud formation and precipitation. There was a minimum uplift of temperature of the order of $\sim 0.15 \text{ }^\circ\text{C}$ corresponding to an increase in ADRF of $\sim 0.35 \text{ W/m}^2$ in the Period 3 of 2019 compared to 2015. The overall temperature was found to increase by $0.43 \text{ }^\circ\text{C}$ with respect to a change in ADRF by $\sim 0.08 \text{ W/m}^2$ in 2019 against the dataset of 2015.

The decline in temperature by $\sim 0.6 \text{ }^\circ\text{C}$ is in accordance with the decrease in ADRF in the Period 1 of 2020 compared to the average of 2015–2019. The temperature in the Period 2 was $31.40 \pm 0.009 \text{ }^\circ\text{C}$ and $30.77 \pm 0.009 \text{ }^\circ\text{C}$ for

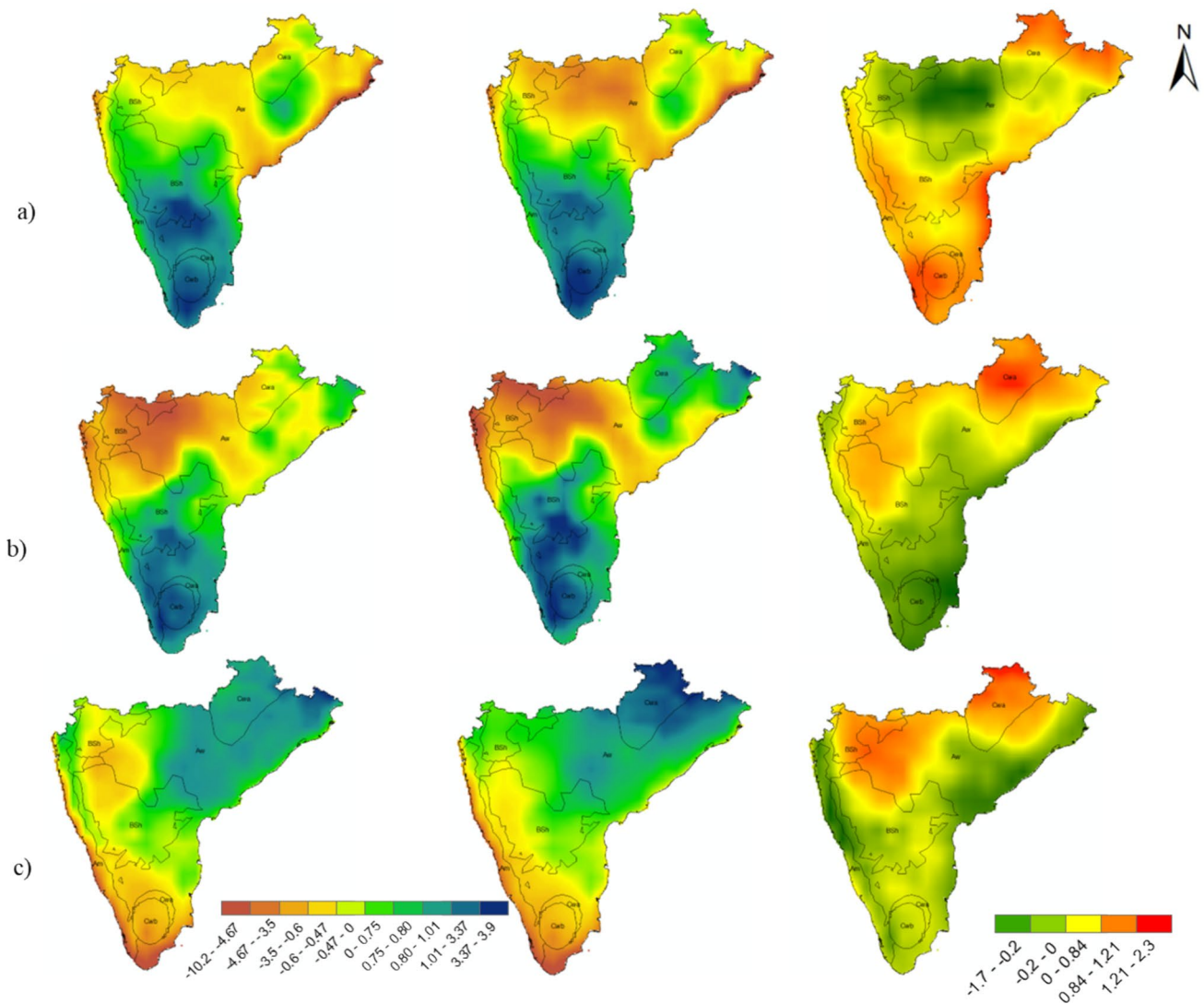


Fig. 7 Spatial distribution of ADRF in the atmosphere for **a** Period 1, **b** Period 2, **c** Period 3 (Left: Average of 2015–2019, Middle: 2020, Right: Change)

the average of 2015–2019 and 2020, respectively. It shows a decrease of $0.63\text{ }^{\circ}\text{C}$, which is contrary to the pattern of ADRF. The Period 3 of 2020 witnessed a mild decrease in temperature by $\sim 0.50\text{ }^{\circ}\text{C}$ compared against the average of 2015–2019. On the contrary, ADRF was found to escalate in the same period. The overall temperature in 2020 was $26.64 \pm 0.004\text{ }^{\circ}\text{C}$ and in the average of 2015–2019 was $27.02 \pm 0.008\text{ }^{\circ}\text{C}$. There was a mild reduction in overall temperature in 2020 which might be attributed to the lockdown restrictions due to the COVID-19 pandemic (Meraj et al., 2021). However, the ADRF was found to uplift by $\sim 1.3\text{W}/\text{m}^2$ in 2020 compared against the average of 2015–2019. This might be due to the entrapment of aerosols in the upper layers of the atmosphere.

During the Period 1, about 56.7% of the study area experienced a decrease in temperature in 2020 compared to the

average of 2015–2019 (Fig. 8). The decrease ranged from 0 to $4.8\text{ }^{\circ}\text{C}$, while the increase in the rest of the study area ranged from 0 to $4.04\text{ }^{\circ}\text{C}$. The decrease was most prominent in Mumbai and Bengaluru that falls in the tropical savanna (Aw) region, as well as a part of the warm semi-arid (BSh) region covering Hyderabad and the humid subtropical (Cwa) region. Nearly, 73% of the study area experienced a decline in temperature during Period 2 in 2020 compared to the average of 2015–2019, with a range of $0\text{--}4.38\text{ }^{\circ}\text{C}$. The remaining part of the study area saw an increase in temperature ranging from 0 to $3.64\text{ }^{\circ}\text{C}$. The increase was most prominent in the warm semi-arid region around Hyderabad and in Goa that falls in the tropical monsoon (Am) region. Meanwhile, the decrease was most prominent in the tropical savanna (Aw) region, as well as a part of the humid subtropical (Cwa) region. During the Period 3, a decrease in

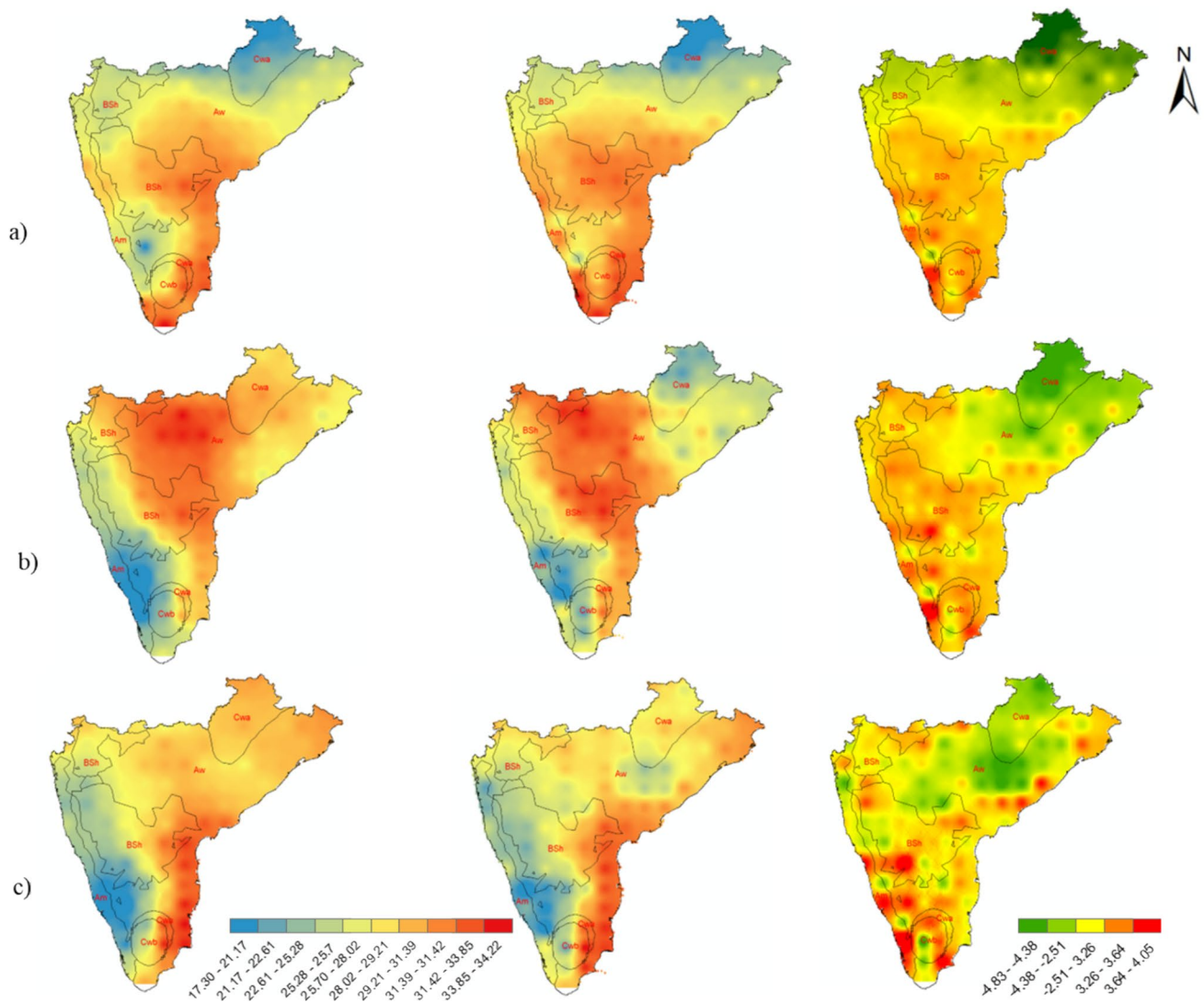


Fig. 8 Spatial distribution of mean temperature for **a** Period 1, **b** Period 2, **c** Period 3 (Left: Avg of 2015–2019, Middle: 2020, Right: Change)

temperature was observed in 85% of the study area, mainly in the tropical savanna (Aw) and humid subtropical (Cwa) regions. The temperature decrease ranged from 0 to 2.51 °C, while the increase in the 15% of the study area ranged from 0 to 3.26 °C. The increase was seen in parts of the tropical monsoon (Am) region, the tropical savanna (Aw) region, and the warm semi-arid (BSh) region.

Conclusions

This study explores the changes in mean temperature due to aerosols in peninsular India over three different analysis periods. The study calculates the ADRF using the proposed factored method and data from the MERRA-2 radiation diagnostics. The Mann–Kendall trend analysis was used to investigate the trend of ADRF over time, and it was found

that ADRF increased from 2015 to 2019, with the highest increase observed in the tropical savanna and warm semi-arid climate regions.

To examine the effect of AOD on temperature, the study analysed the variables for the three analysis periods in 2020 and compared them to the average values from 2015 to 2019. The findings showed that during the pre-lockdown phase, AOD, ADRF, and mean temperature reduced, with the tropical savanna region experiencing the biggest decline. This indicates that aerosols have a cooling effect on the atmosphere.

However, the Period 2 of 2020 has witnessed a decrease in AOD and mean temperature while ADRF increased in most of the study area. The increase in ADRF may be attributed to energy being trapped in the upper layers of the atmosphere. The same pattern was observed in the Period 3. These findings suggest that the relationship between AOD

and other climate variables in peninsular India can impact weather processes and the onset of the south-west monsoon (Sarangi et al., 2016, Niyogi et al., 2007). This analysis can also be extended to examine the increase in thunderstorms and precipitation after the lifting of restrictions in the study area.

In conclusion, this study's findings provide valuable information on the effect of aerosols on temperature in peninsular India over different analysis periods. The study highlights the importance of understanding the relationship between aerosols and other climate variables, which can provide insights into the onset of the south-west monsoon and weather processes in the region. Further research in this area can help us to better understand and mitigate the impacts of climate change on the region.

Acknowledgements The corresponding author's (V. Sridhar) effort was funded in part by the Virginia Agricultural Experiment Station (Blacksburg) and through the Hatch Program of the National Institute of Food and Agriculture at the United States Department of Agriculture (Washington, DC) and as a Fulbright- Nehru senior scholar funded by the United States India Educational Foundation.

Author's contribution Tharani Kotrike (TK) Conceptualization; Data curation; Formal analysis; Investigation; Software; Writing—original draft; review & editing; Venkata Reddy Keesara (VRK) Conceptualization; Data curation; Investigation; Methodology; Supervision; Resources; Writing—original draft; review & editing; Venkataramana Sridhar (VS) Conceptualization; Data curation; Methodology; Supervision; Validation; Visualization; Roles/Writing—original draft; Writing—review & editing; Deva Pratap (DP) Data curation; Methodology; Validation; Visualization; Supervision; Resources; Roles/Writing—original draft.

Funding Not applicable.

Declarations

Conflict of Interest The authors declared that they have no conflict of interest.

Open Access This article is licensed under a Creative Commons Attribution 4.0 International License, which permits use, sharing, adaptation, distribution and reproduction in any medium or format, as long as you give appropriate credit to the original author(s) and the source, provide a link to the Creative Commons licence, and indicate if changes were made. The images or other third party material in this article are included in the article's Creative Commons licence, unless indicated otherwise in a credit line to the material. If material is not included in the article's Creative Commons licence and your intended use is not permitted by statutory regulation or exceeds the permitted use, you will need to obtain permission directly from the copyright holder. To view a copy of this licence, visit <http://creativecommons.org/licenses/by/4.0/>.

References

- Allen, S. K., Plattner, G. K., Nauels, A., Xia, Y., & Stocker, T.F. (2014). Climate change 2013: The physical science basis. An overview of the Working Group 1 contribution to the Fifth Assessment Report of the Intergovernmental Panel on Climate Change (IPCC). In *EGU general assembly conference abstracts* (p. 3544).
- Anil, S., Manikanta, V., & Pallakury, A. R. (2021). Unravelling the influence of subjectivity on ranking of CMIP6 based climate models: A case study. *International Journal of Climatology*, 41(13), 5998–6016.
- Bellouin, N., Quaas, J., Gryspeerdt, E., Kinne, S., Stier, P., Watson-Parris, D., Stevens, B. (2020). Bounding global aerosol radiative forcing of climate change. *Reviews of Geophysics*, 58(1), e2019RG000660.
- Buchard, V., Randles, C. A., Da Silva, A. M., Darmenov, A., Colarco, P. R., Govindaraju, R. & Yu, H. (2017). The MERRA-2 aerosol reanalysis, 1980 onward. Part II: Evaluation and case studies. *Journal of Climate*, 30(17), 6851–6872.
- Chakraborty, A., Kumar Das, P., Sessa Sai, M.V.R. & Behera, G., (2012). Spatial pattern of temporal trend of crop phenology matrices over india using timeseries gimms NDVI data (1982–2006). *The International Archives of the Photogrammetry, Remote Sensing and Spatial Information Sciences*, 38, 113–118
- Cheng, F., Zhang, J., He, J., Zha, Y., Li, Q., & Li, Y. (2017). Analysis of aerosol-cloud-precipitation interactions based on MODIS data. *Advances in Space Research*, 59(1), 63–73.
- Das, S., Dey, S., & Dash, S. K. (2015). Impacts of aerosols on dynamics of Indian summer monsoon using a regional climate model. *Climate Dynamics*, 44, 1685–1697.
- Evans, J. S., Murphy, M. A. (2019). spatialEco. R package version 2.0-2
- Fawole, O. G., Cai, X., Pinker, R. T., & MacKenzie, A. R. (2019). Analysis of radiative properties and direct radiative forcing estimates of dominant aerosol clusters over an urban-desert region in West Africa. *Aerosol and Air Quality Research*, 19(1), 38–48.
- Gouda, K. C., Gogeri, I., & ThippaReddy, A. S. (2022). Assessment of aerosol optical depth over Indian subcontinent during COVID-19 lockdown (March–May 2020). *Environmental Monitoring and Assessment*, 194(3), 195.
- <https://mausam.imd.gov.in>
- Irfan, M., Razzaq, A., Suksatan, W., Sharif, A., Elavarasan, R. M., Yang, C. & Rauf, A. (2022). Asymmetric impact of temperature on COVID-19 spread in India: Evidence from quantile-on-quantile regression approach. *Journal of Thermal Biology*, 104, 103101.
- Jaksa, W. T., Sridhar, V., Huntington, J. L., & Khanal, M. (2013). Evaluation of the complementary relationship using Noah land surface model and North American regional reanalysis (NARR) data to estimate evapotranspiration in semiarid ecosystems. *Journal of Hydrometeorology*, 14(1), 345–359.
- Kendall, M. G. (1975). Rank Correlation Methods. 4th edition, Charles Griffin, London, UK
- Kotrike, T., Pratap, D., & Keesara, V. R. (2021). Validation and trend analysis of satellite-based AOD data over Southern India. *Aerosol Science and Engineering*, 5, 32–43.
- Kumar, G., Madhavan, B. L., Sahu, L. K., Kumar, Y. B., Vernier, J. P., Liu, H. & Sinha, P. R. (2023). Multi-year CALIPSO observations of ubiquitous elevated aerosol layer in the free troposphere over South Asia: Sources and formation mechanism. *Journal of Geophysical Research: Atmospheres*, 128(2), e2012JD6277.
- Kumar, M., Parmar, K. S., Kumar, D. B., Mhawish, A., Broday, D. M., Mall, R. K., & Banerjee, T. (2018). Long-term aerosol climatology over Indo-Gangetic Plain: Trend, prediction and potential source fields. *Atmospheric Environment*, 180, 37–50.
- Li, J., & Tartarini, F. (2020). Changes in air quality during the COVID-19 Lockdown in Singapore and associations with human mobility trends. *Aerosol and Air Quality Research*, 20(8), 1748–1758.
- Li, Z., Guo, J., Ding, A., Liao, H., Liu, J., Sun, Y. & Zhu, B. (2017). Aerosol and boundary-layer interactions and impact on air quality. *National Science Review*, 4(6), 810–833.

- Liu, S., Xing, J., Zhao, B., Wang, J., Wang, S., Zhang, X., & Ding, A. (2019). Understanding of aerosol–climate interactions in China: Aerosol impacts on solar radiation, temperature, cloud, and precipitation and its changes under future climate and emission scenarios. *Current Pollution Reports*, 5, 36–51.
- Liu, Z., Yim, S. H., Wang, C., & Lau, N. C. (2018). The impact of the aerosol direct radiative forcing on deep convection and air quality in the Pearl River Delta region. *Geophysical Research Letters*, 45(9), 4410–4418.
- López-Romero, J. M., Montávez, J. P., Jerez, S., Lorente-Plazas, R., Palacios-Peña, L., & Jiménez-Guerrero, P. (2021). Precipitation response to aerosol–radiation and aerosol–cloud interactions in regional climate simulations over Europe. *Atmospheric Chemistry and Physics*, 21(1), 415–430.
- Mann, H. B. (1945). Nonparametric tests against trend. *Econometrica Journal of the Econometric Society*, pp. 245–259.
- Manoj, M. R., Satheesh, S. K., Moorthy, K. K., Gogoi, M. M., & Babu, S. S. (2019). Decreasing trend in black carbon aerosols over the Indian region. *Geophysical Research Letters*, 46(5), 2903–2910.
- Mao, Q., & Wan, H. (2022). Study on the characteristics of aerosol radiative forcing under complex pollution conditions in Beijing. *Atmosphere*, 13(3), 501.
- Menon, H. B., Shirodkar, S., Kedia, S., Ramachandran, S., Babu, S., & Moorthy, K. K. (2014). Temporal variation of aerosol optical depth and associated shortwave radiative forcing over a coastal site along the west coast of India. *Science of the Total Environment*, 468, 83–92.
- Meraj, G., Farooq, M., Singh, S. K., Romshoo, S. A., Sudhanshu., Nathawat, M.S. & Kanga, S.. (2021). Coronavirus pandemic versus temperature in the context of Indian subcontinent: A preliminary statistical analysis. *Environment, Development and Sustainability*, 23, 6524–6534.
- Muhammad, S., Long, X. & Salman, M., (2020). COVID-19 pandemic and environmental pollution: A blessing in disguise?. *Science of the total environment*, 728, 138820
- Navinya, C., Patidar, G., & Phuleria, H. C. (2020). Examining effects of the COVID-19 national lockdown on ambient air quality across urban India. *Aerosol and Air Quality Research*, 20(8), 1759–1771.
- Niyogi, D., Chang, H. I., Chen, F., Gu, L., Kumar, A., Menon, S., & Pielke, R. A. (2007). Potential impacts of aerosol–land–atmosphere interactions on the Indian monsoonal rainfall characteristics. *Natural Hazards*, 42, 345–359.
- Pandey, S. K., Vinoj, V., & Panwar, A. (2020). The short-term variability of aerosols and their impact on cloud properties and radiative effect over the Indo-Gangetic Plain. *Atmospheric Pollution Research*, 11(3), 630–638.
- Paulot, F., Paynter, D., Ginoux, P., Naik, V., & Horowitz, L. W. (2018). Changes in the aerosol direct radiative forcing from 2001 to 2015: Observational constraints and regional mechanisms. *Atmospheric Chemistry and Physics*, 18(17), 13265–13281.
- Penna, B., Herdies, D., & Costa, S. (2018). Estimates of direct radiative forcing due to aerosols from the MERRA-2 reanalysis over the Amazon region. *Atmospheric Chemistry and Physics Discussions*, 2018, 1–17.
- Putaud, J.P., Cavalli, F., Martins dos Santos, S. & Dell’Acqua, A., (2014). Long-term trends in aerosol optical characteristics in the Po Valley, Italy. *Atmospheric Chemistry and Physics*, 14(17), 9129–9136
- Ramanathan, V., Chung, C., Kim, D., Bettge, T., Buja, L., Kiehl, J. T. & Wild, M. (2005). Atmospheric brown clouds: Impacts on South Asian climate and hydrological cycle. *Proceedings of the National Academy of Sciences*, 102(15), 5326–5333.
- Rana, A., Jia, S., & Sarkar, S. (2019). Black carbon aerosol in India: A comprehensive review of current status and future prospects. *Atmospheric Research*, 218, 207–230.
- Rani, S., & Kumar, R. (2022). Spatial distribution of aerosol optical depth over India during COVID-19 lockdown phase-1. *Spatial Information Research*, 30(3), 417–426.
- Remer, L. A., Kaufman, Y. J., Tanré, D., Mattoo, S., Chu, D. A., Martins, J. V. & Holben, B. N. (2005). The MODIS aerosol algorithm, products, and validation. *Journal of the Atmospheric Sciences*, 62(4), 947–973.
- Rienecker, M. M., Suarez, M. J., Gelaro, R., Todling, R., Bacmeister, J., Liu, E., & Woollen, J. (2011). MERRA - NASA’s modern-era retrospective analysis for research and applications. *Journal of Climate*, 24(14), 3624–3648.
- Rosenfeld, D., Lohmann, U., Raga, G. B., O’Dowd, C. D., Kulmala, M., Fuzzi, S. & Andreae, M. O. (2008). Flood or drought: How do aerosols affect precipitation? *Science*, 321(5894), 1309–1313.
- Rutan, D. A., Kato, S., Doelling, D. R., Rose, F. G., Nguyen, L. T., Caldwell, T. E., & Loeb, N. G. (2015). CERES synoptic product: Methodology and validation of surface radiant flux. *Journal of Atmospheric and Oceanic Technology*, 32(6), 1121–1143.
- Sahu, L. K., Tripathi, N., Gupta, M., Singh, V., Yadav, R., & Patel, K. (2022). Impact of COVID-19 pandemic lockdown in ambient concentrations of aromatic volatile organic compounds in a metropolitan city of western India. *Journal of Geophysical Research: Atmospheres*, 127(6), e2022JD036628.
- Sarang, C., Tripathi, S. N., Mishra, A. K., Goel, A., & Welton, E. J. (2016). Elevated aerosol layers and their radiative impact over Kanpur during monsoon onset period. *Journal of Geophysical Research: Atmospheres*, 121(13), 7936–7957.
- Sarkar, S., Chokngamwong, R., Cervone, G., Singh, R. P., & Kafatos, M. (2006). Variability of aerosol optical depth and aerosol forcing over India. *Advances in Space Research*, 37(12), 2153–2159.
- Satheesh, S.K. (2002). Letter to the Editor Aerosol radiative forcing over land: Effect of surface and cloud reflection. In *Annales Geophysicae* (Vol. 20, No. 12, pp. 2105–2109). Göttingen, Germany: Copernicus Publications.
- Sehgal, V., Sridhar, V. (2019). Watershed-scale retrospective drought analysis and seasonal forecasting using multi-layer, high-resolution simulated soil moisture for Southeastern U.S., *Weather and Climate Extremes*, 23, 100191
- Setti, S., Maheswaran, R., Radha, D., Sridhar, V., Barik, K. K., & Narasimham, M. L. (2020). Attribution of hydrologic changes in a tropical river basin to climate and land use change: A case study from India. *Journal of Hydrologic Engineering*. 25(8), 05020015
- Shonk, J. K., Turner, A. G., Chevuturi, A., Wilcox, L. J., Dittus, A. J., & Hawkins, E. (2020). Uncertainty in aerosol radiative forcing impacts the simulated global monsoon in the 20th century. *Atmospheric Chemistry and Physics*, 20(23), 14903–14915.
- Singh, R. P., & Chauhan, A. (2020). Impact of lockdown on air quality in India during COVID-19 pandemic. *Air Quality, Atmosphere & Health*, 13(8), 921–928.
- Sridhar, V., & Anderson, K. A. (2017). Human-induced modifications to boundary layer fluxes and their water management implications in a changing climate. *Agricultural and Forest Meteorology*, 234, 66–79.
- Sridhar, V., Billah, M., & Valayamkunnath, P. (2018). Field-scale intercomparison analysis of ecosystems in partitioning surface energy balance components in a semi-arid environment. *Ecology and Hydrobiology*. 19(1), 24–37
- Sridhar, V., & Elliott, R. L. (2002). On the development of a simple downwelling longwave radiation scheme. *Agricultural and Forest Meteorology*, 112(3–4), 237–243.
- Sridhar, V., & Wedin, D. A. (2009). Hydrological behavior of grasslands of the Sandhills: Water and energy balance assessment from measurements. *Treatments and Modeling, Ecohydrology*, 2, 195–212. <https://doi.org/10.1002/eco.61>

- Srivastava, A. K., Rajeevan, M., & Kshirsagar, S. R. (2009). Development of high resolution daily gridded temperature data set (1969–2005) for the Indian region. *Atmospheric Science Letters*. <https://doi.org/10.1002/asl.232>
- Srivastava, A. K., Bhoyar, P. D., Kanawade, V. P., Devara, P. C., Thomas, A., & Soni, V. K. (2021). Improved air quality during COVID-19 at an urban megacity over the Indo-Gangetic Basin: From stringent to relaxed lockdown phases. *Urban Climate*, 36, 100791.
- Srivastava, R. (2017). Trends in aerosol optical properties over South Asia. *International Journal of Climatology*, 37(1), 371–380.
- Subba, T., Gogoi, M. M., Pathak, B., Bhuyan, P. K., & Babu, S. S. (2020). Recent trend in the global distribution of aerosol direct radiative forcing from satellite measurements. *Atmospheric Science Letters*, 21(11), e975.
- Thomas, G., Thomas, J., Mathew, A.V., Devika, R.S., Krishnan, A., & Nair, A.J., 2022. Non-uniform effect of COVID-19 lockdown on the air quality in different local climate zones of the urban region of Kochi, India. *Spatial Information Research*, 31(2), 145–155.
- Thomas, A., Kanawade, V. P., Sarangi, C., & Srivastava, A. K. (2021). Effect of COVID-19 shutdown on aerosol direct radiative forcing over the Indo-Gangetic Plain outflow region of the Bay of Bengal. *Science of the Total Environment*, 782, 146918.
- Tobias, A., Carnerero, C., Reche, C., Massagué, J., Via, M., Minguilon, M. C. & Querol, X. (2020). Changes in air quality during the lockdown in Barcelona (Spain) one month into the SARS-CoV-2 epidemic. *Science of the Total Environment*, 726, 138540.
- Valayamkunnath, P., Sridhar, V., Zhao, W., & Allen, R. G. (2018). Intercomparison of surface energy fluxes, soil moisture, and evapotranspiration from eddy covariance, large aperture scintillometer, and modeling across three ecosystems in a semiarid climate. *Agricultural and Forest Meteorology*, 248, 22–47.
- Vijayakumar, K., Devara, P. C. S., Giles, D. M., Holben, B. N., & S. Vijaya Bhaskara Rao & C. K. Jayasankar., (2018). Validation of satellite and model aerosol optical depth and precipitable water vapour observations with AERONET data over Pune India. *International Journal of Remote Sensing*, 39(21), 7643–7663.
- Wang, J., Dong, J., Yi, Y., Lu, G., Oyler, J., Smith, W. K. & Running, S., (2017). Decreasing net primary production due to drought and slight decreases in solar radiation in China from 2000 to 2012. *Journal of Geophysical Research: Biogeosciences*, 122(1), 261–278
- Woodward, A., Smith, K. R., Campbell-Lendrum, D., Chadee, D. D., Honda, Y., Liu, Q. & Haines, A. (2014). Climate change and health: On the latest IPCC report. *The Lancet*, 383(9924), 1185–1189.
- Yang, Y., Wang, H., Smith, S. J., Zhang, R., Lou, S., Yu, H. & Rasch, P. J. (2018). Source apportionments of aerosols and their direct radiative forcing and long-term trends over continental United States. *Earth's Future*, 6(6), 793–808.
- Yu, H., Kaufman, Y. J., Chin, M., Feingold, G., Remer, L. A., Anderson, T. L., Balkanski, Y., Bellouin, N., Boucher, O., Christopher, S., & DeCola, P. (2006). A review of measurement-based assessments of the aerosol direct radiative effect and forcing. *Atmospheric Chemistry and Physics*, 6(3), 613–666.
- Zalakeviciute, R., Vasquez, R., Bayas, D., Buenano, A., Mejia, D., Zegarra, R. & Lamb, B. (2020). Drastic improvements in air quality in Ecuador during the COVID19 outbreak. *Aerosol Air Quality Research*, 20, 1783–1792.
- Zhang, J., Christopher, S.A., Remer, L.A. and Kaufman, Y.J., 2005. Shortwave aerosol radiative forcing over cloud-free oceans from Terra: 2. Seasonal and global distributions. *Journal of Geophysical Research: Atmospheres*, 110(D10).

Publisher's Note Springer Nature remains neutral with regard to jurisdictional claims in published maps and institutional affiliations.